Journal of Experimental Nanoscience
Publication details, including instructions for authors and subscription information:
http://www.informaworld.com/smpp/title~content=t716100757

pH-dependent adsorption of Au nanoparticles on chemically modified Si_3N_4 MEMS devices

C. A. E. Hamlett[a]; P. T. Docker[b]; M. C. L. Ward[b]; P. D. Prewett[b]; K. Critchley[c]; S. D. Evans[c]; J. A. Preece[a]
[a] School of Chemistry, University of Birmingham, Birmingham, B15 2TT, UK [b] School of Mechanical Engineering, University of Birmingham, Birmingham, B15 2TT, UK [c] School of Physics and Astronomy, University of Leeds, Leeds, LS2 9JT, UK

To cite this Article Hamlett, C. A. E. , Docker, P. T. , Ward, M. C. L. , Prewett, P. D. , Critchley, K. , Evans, S. D. and Preece, J. A.(2009) 'pH-dependent adsorption of Au nanoparticles on chemically modified Si_3N_4 MEMS devices', Journal of Experimental Nanoscience, 4: 2, 147 — 157
To link to this Article: DOI: 10.1080/17458080902929911
URL: http://dx.doi.org/10.1080/17458080902929911

Journal of Experimental Nanoscience
Vol. 4, No. 2, June 2009, 147–157

Taylor & Francis
Taylor & Francis Group

pH-dependent adsorption of Au nanoparticles on chemically modified Si_3N_4 MEMS devices

C.A.E. Hamlett[a], P.T. Docker[b]†, M.C.L. Ward[b], P.D. Prewett[b], K. Critchley[c]‡, S.D. Evans[c] and J.A. Preece[a]*

[a]*School of Chemistry, University of Birmingham, Edgbaston, Birmingham, B15 2TT, UK;* [b]*School of Mechanical Engineering, University of Birmingham, Edgbaston, Birmingham, B15 2TT, UK;* [c]*School of Physics and Astronomy, University of Leeds, Leeds, LS2 9JT, UK*

(*Received 14 January 2009; final version received 28 March 2009*)

Microelectromechanical systems (MEMS) are devices that represent the integration of mechanical and electrical components in the micrometer regime. Self-assembled monolayers (SAMs) can be used to functionalise the surface of MEMS resonators in order to fabricate chemically specific mass sensing devices. The work carried out in this article uses atomic force microscopy (AFM) and X-ray photoemission spectroscopy (XPS) data to investigate the pH-dependent adsorption of citrate-passivated Au nanoparticles to amino-terminated Si_3N_4 surfaces. AFM, XPS and mass adsorption experiments, using 'flap' type resonators, show that the maximum adsorption of nanoparticles takes place at pH = 5. The mass adsorption data, obtained using amino functionalised 'flap' type MEMS resonators, shows maximum adsorption of the Au nanoparticles at pH = 5 which is in agreement with the AFM and XPS data, which demonstrates the potential of such a device as a pH responsive nanoparticle detector.

Keywords: pH-dependent adsorption; MEMS; gold nanoparticles; sensors

1. Introduction

Microelectromechanical systems (MEMS) devices are defined by the integration of electrical and mechanical components on the micron length scale [1]. Examples of the use of MEMS devices include actuators [2,3] and sensors [4–14]. MEMS devices can be used as chemical sensors *via* mass detection [7,14], whereby the resonant frequency of a MEMS resonator changes upon the adsorption of chemical species; the resultant change of resonant frequency is proportional to the mass adsorbed on the surface [4,7,15]. Hence, the mass of the adsorbed species can be calculated using knowledge of the mass sensitivity of the device. Such devices operate on a similar principle to both quartz crystal microbalances (QCM) [16,17] and surface acoustic wave (SAW) devices [18,19].

*Corresponding author. Email: j.a.preece@bham.ac.uk
†Present address: Department of Chemistry, The University of Hull, UK.
‡Present address: The Department of Chemical Engineering, University of Michigan, USA.

ISSN 1745–8080 print/ISSN 1745–8099 online

DOI: 10.1080/17458080902929911
http://www.informaworld.com

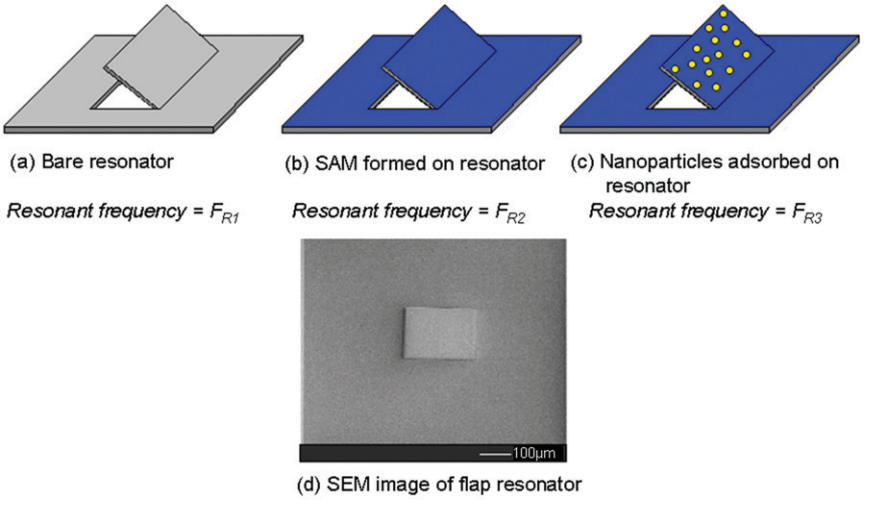

Figure 1. (a)–(c) An overview of the mass-detection of Au nanoparticles on chemically modified Si_3N_4 'flap' resonators and the frequencies measured in order to calculate mass adsorption; (d) an SEM image of the 'flap' type resonator.

The species adsorbed on the surface of MEMS mass detection devices is dictated by the surface chemistry of the resonator with self-assembled monolayers (SAMs) having been employed to immobilise specific species to the MEMS sensors [5,7–9,12].

The aim of the research described in this article is to demonstrate the pH-dependent immobilisation of citrate-passivated Au nanoparticles to amino-functionalised Si_3N_4 surfaces with a view to transferring such surface chemistry to a MEMS resonator. Previous work has shown pH-dependent adsorption of citrate-passivated Au nanoparticles to aromatic amino-functionalised Au [20] and aliphatic amino-functionalised SiO_2 [21] substrates. The investigation of the pH-dependent adsorption of citrate-passivated Au nanoparticles to aliphatic amino-functionalised Si_3N_4 substrates will provide a model system with which the pH-dependent adsorption of nanoparticles to MEMS devices can be tested. Atomic force microscopy (AFM) and X-ray photoemission spectroscopy (XPS) data will be used to determine the maximum pH at which citrate-passivated Au nanoparticles attach to $-NH_2$-functionalised Si_3N_4 substrates. Thus, providing both (i) a reference of the pH-dependent adsorption of citrate-passivated Au nanoparticles to Si_3N_4 resonators modified with 3-aminopropyltrimethoxysilane (APTMS) SAMs, and (ii) a model system to show that such chemically modified microresonators can be used as mass sensors for nanoparticles (Figure 1).

2. Results and discussion

AFM and XPS analysis have been used to monitor the pH-dependent adsorption of citrate-passivated nanoparticles on Si_3N_4 substrates modified by exposure to APTMS vapour. We have described the formation of thin films of APTMS by a vapour method onto Si_3N_4, previously [22]. Here, we report the pH-dependent adsorption of citrate-passivated Au nanoparticles on these films by monitoring with AFM (surface coverage),

XPS (elemental composition) and MEMS resonators (mass adsorption, see Figure 1). All three techniques reveal a peak adsorption at pH = 5.

2.1. *Au nanoparticle adsorption studies*

AFM images were obtained from Si_3N_4 substrates, modified with APTMS SAMs, after immersion for 2 h in aqueous solutions of citrate-passivated Au nanoparticles at five different values of pH (pH = 3, 4, 5, 6 and 7) (Figure 2(a)). A graph of nanoparticle surface coverage versus the pH is shown in Figure 3 (block circles).

At pH values of 3 and 4 it can be seen that the occurrence of Au nanoparticle aggregates adsorbed on the surface is more pronounced than at pH = 5, 6 or 7 (Figure 2(a)). Presumably, the occurrence of a higher degree of nanoparticulate aggregates at pH values of 3 and 4, compared to pH values 5, 6 or 7, is due to a higher degree of protonation of the passivating citrate anions in solution, corresponding to a lower degree of electrostatic repulsion between the particles, leading to gold core fusion. The reduction of the number of repulsive negative charges on citrate-passivated Au nanoparticles at acidic pHs has previously been demonstrated by zeta potentiometry [21]. The maximum adsorption of citrate-passivated Au nanoparticles occurs at pH=5 (Figures 2(a) and 3), which is consistent with previous work which shows that optimal adsorption of citrate-passivated Au nanoparticles on $-NH_2$ terminated SAMs on SiO_2 substrates occurs at pH ~ 5 [21].

XPS spectra of APTMS-modified Si_3N_4 substrates were recorded after immersion in solutions of citrate-passivated Au nanoparticles over the pH range 3–7. The Au 4f spectra (Figure 2(b)) and Si 2p spectra, shown in Figure A1 (see Appendix), were used to calculate the Au/Si ratio in order to determine the relative change of nanoparticle adsorption. The Au/Si ratios were used to study the adsorption of Au nanoparticles using the Si substrate as an internal standard, assuming that the amount of Si present is constant. Figure 3 (open squares) shows that the maximum Au/Si ratio occurs at pH ~ 5 which shows that the maximum nanoparticle adsorption occurs at pH ~ 5. This result concurs with the AFM data (Figure 3 (closed circles)).

When nanoparticle adsorption is carried out at pH = 5, 6 and 7 the Au 4f spectra appear as two distinct peaks (the Au $4f_{5/2}$ and Au $4f_{7/2}$ peaks). However, when nanoparticle adsorption is carried out at pH = 3 and 4 the Au 4f peaks appear to split (Figure 2(a)) and this coincides with the aggregation of Au nanoparticles (Figure 2(b)). The binding energy of the Au $4f_{7/2}$ for Au^{3+} occurs at 86.7 eV [23] and one of the split Au $4f_{7/2}$ peaks shifts towards this value. Therefore, this indicates that at pH = 3 and 4 the citrate-passivated Au nanoparticles are partially oxidised. Praharaj et al. [24] have observed that the addition of HCl to Au nanoparticles can lead to the oxidation of Au^0 to Au^{3+} and HCl is used for the reduction of pH of the Au nanoparticle solution in this study. Therefore, the splitting of the Au 4f peaks by XPS is presumably due to the oxidation of the Au.

Both AFM and XPS measurements demonstrate that maximum Au nanoparticle adsorption to an APTMS thin film occurs at pH = 5 (Figure 3). To rationalise this observation we need to consider the pK_a of the surface-active components. The pK_a of aliphatic amine groups is 8–11 in free solution [25]; however, when attached to a surface

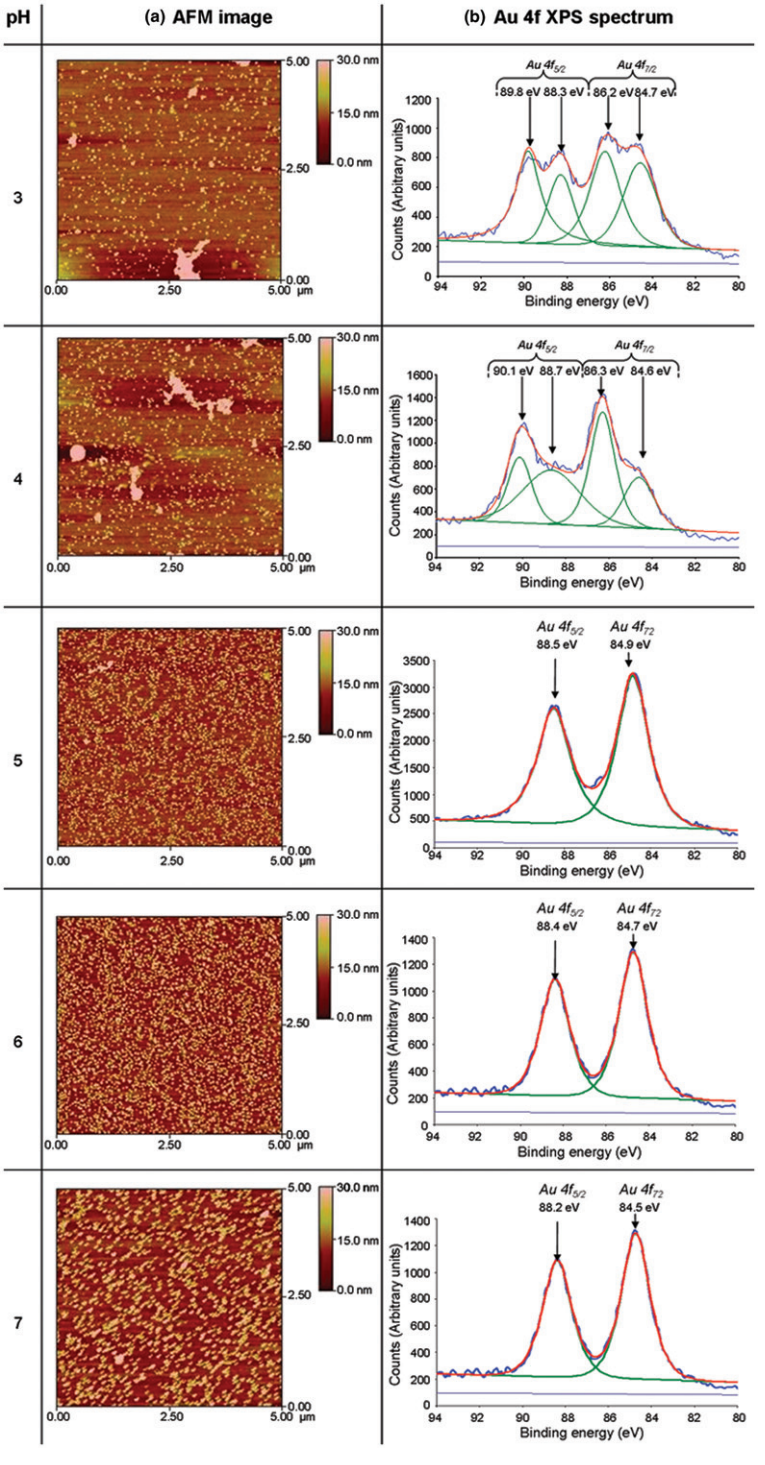

Figure 2. AFM images and XPS Au 4f spectra of adsorption of citrate-passivated Au nanoparticles on APTMS-modified Si_3N_4 substrates at five different values of pH. The binding energies of both the Au $4f_{5/2}$ and Au $4f_{7/2}$ XPS peaks and peak fitting of the XPS spectra are also shown.

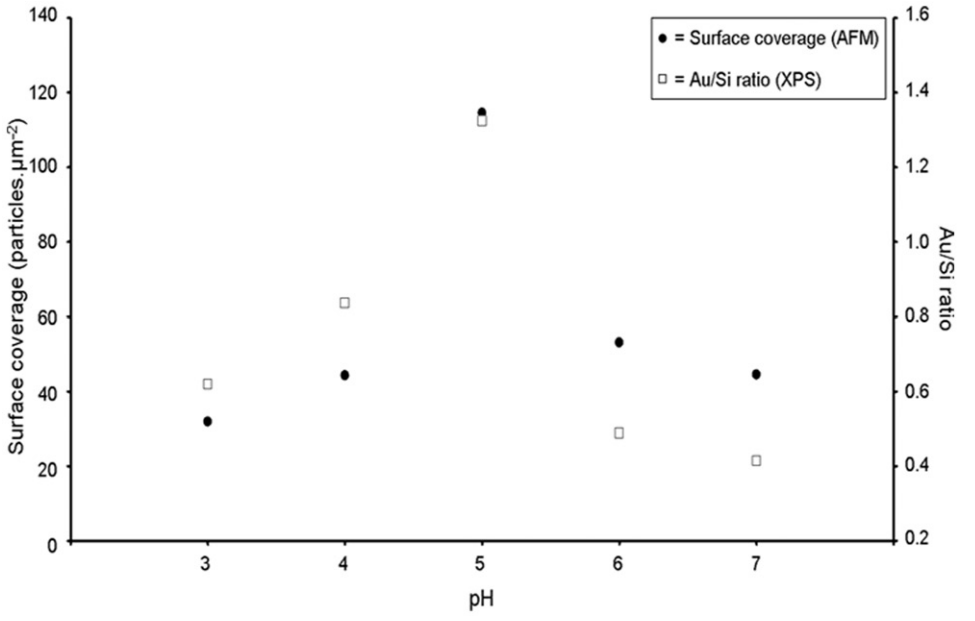

Figure 3. Graph showing both particle density (measured by AFM) and Au/Si ratio (measured by XPS) *vs.* pH of citrate-passivated Au nanoparticles adsorbed onto APTMS-modified Si_3N_4 substrates.

the pK_a decreases to 6–8 [26]. The pK_a of COOH groups in free solution is ~4.8 [27] and we might expect a shift to lower pK_a on the surface of the Au nanoparticles. Thus, at pH values of 3 and 4 few COOH groups will be deprotonated, hence, there will be little or no repulsive electrostatic forces existing between the particles, leading to aggregation of the nanoparticles (Figure 4). Furthermore, the neutral Au nanoparticles do not lend themselves to electrostatic attachment to the positively charged APTMS SAMs (although hydrogen bonding will occur). The maximum adsorption of Au nanoparticles occurs at pH = 5, which is due to the best balance between the citrate-passivated nanoparticles being negatively charged and the amino surface being positively charged (Figure 4). However, at pH = 6 and 7 nanoparticle adsorption reduces as the APTMS thin film becomes increasingly deprotonated at a rate greater than that at which the Au nanoparticles become negatively charged (Figure 4). Therefore, the electrostatic attraction between the negatively charged Au nanoparticles and the APTMS surface decreases due to a less positively charged surface as the pH increases.

2.2. *Mass adsorption measurements*

Initial mass adsorption measurements were made by measuring the frequency shift of simple 'flap' type resonators (Figure 1 and Table A1) at three different pH values. These MEMS devices were fabricated using focused ion beam (FIB) microfabrication to cut a flap with three free sides from a membrane of silicon nitride, 500 nm thick. Each device measures approximately $200 \times 150\ \mu m^2$ and is designed to oscillate in 'flap mode' about an

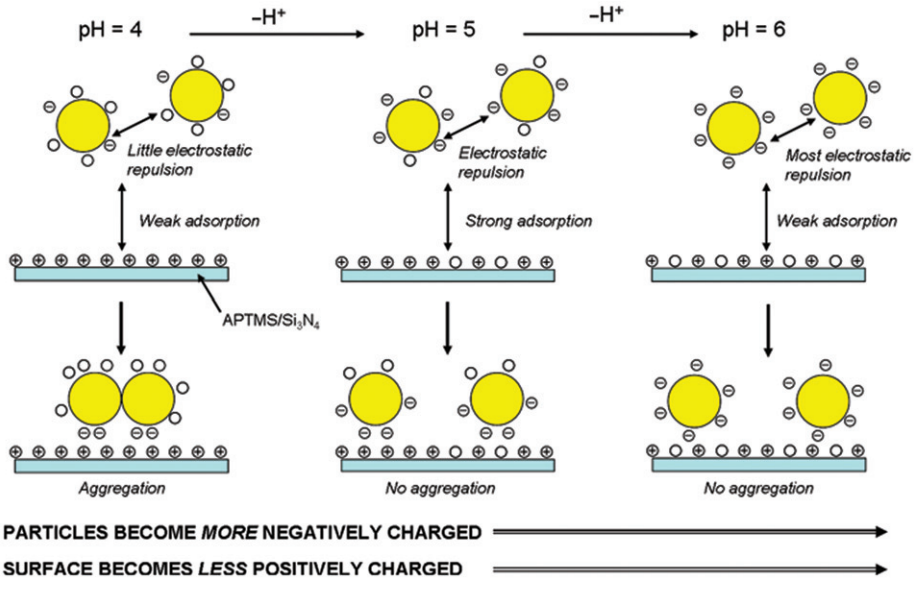

Figure 4. Schematic representation of the charges present on the citrate-passivated Au nanoparticles and APTMS surface at three different values of pH (pH = 4, 5 and 6) and the subsequent deposition of Au nanoparticles on and APTMS thin film.

axis of rotation through the fixed side. The devices were excited by mounting them on a piezoelectric chip in an SEM, which was connected to a vibrometer. Careful tuning of the drive frequency of the piezoelectric crystal, coupled with real time observation under the SEM, allowed the resonant frequency to be found once the edge of the flap became blurred.

The devices were calculated to have a frequency shift of 590 Hz/10^{-8} g using MathCAD software. Therefore, this value was used to calculate the masses adsorbed on the resonators once the frequency shift was determined. The results shown in Figure 5 indicate maximum nanoparticle adsorption at pH = 5, in agreement with the AFM and XPS data (Figure 3) though the difference in absorbance between pH = 5 and 6 is not as pronounced as that in Figure 3.

3. Conclusions

The aim of the work presented in this article is to show that the pH-dependent adsorption of citrate-passivated Au nanoparticles on amino-functionalised Si_3N_4 resonators can be used as a model system for the development of MEMS nanoparticulate sensors (Figure 1). AFM (Figure 2(a)), XPS (Figure 2(b)) and mass detection, using chemically modified resonators (Figures 1 and 5), was used to monitor the pH-dependent adsorption of citrate-passivated Au nanoparticles on amino-functionalised Si_3N_4 surfaces. AFM images (Figure 2(a)) reveal that the Au nanoparticles form aggregates on the APTMS surface at pH = 3 and 4. This observation is due to the loss of electrostatic repulsion between the particles as a result of decreased deprotonation of the COOH moieties on

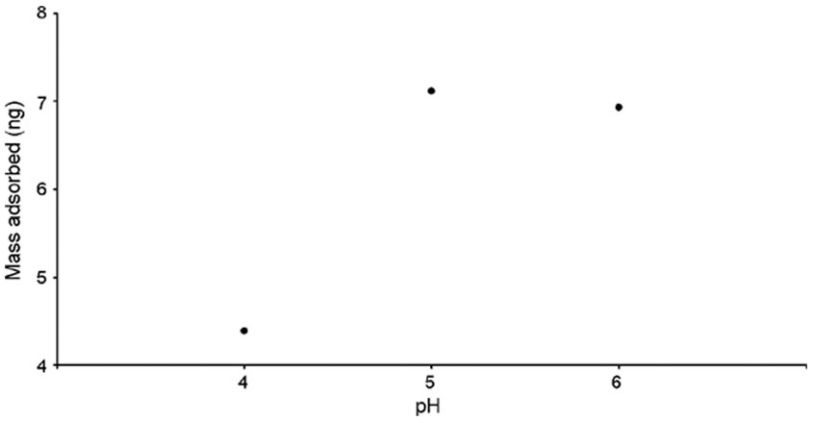

Figure 5. Graph showing the mass of citrate-passivated Au nanoparticles adsorbed on APTMS-modified Si_3N_4 'flap' resonators *vs.* pH.

the nanoparticles at pH = 3 and 4 (Figure 4). Maximum surface coverage of nanoparticles was observed at pH = 5 (Figures 2(a) and 3 (block circles)) when the balance between electrostatic repulsion between the Au nanoparticles and the degree of protonation of the APTMS surface is optimal (Figure 4). At pH = 6 and 7 the degree of surface coverage (Figures 2(a) and 3 (block circles)) is less than at pH = 5, which is due to a decrease in surface protonation at higher values of pH compared to that at pH = 5 (Figure 4). XPS analysis (Figure 2(b)) was used to calculate the Au/Si ratio which, in agreement with the surface coverage calculated by AFM, shows maximum Au coverage at pH = 5 (Figure 3 (open squares)). XPS also reveals splitting of both the Au $4f_{5/2}$ and Au $4f_{7/2}$ peaks, which is representative of oxidation of the Au nanoparticles. Such peak splitting was not observed when particle absorption was carried out at pH = 5, 6 or 7, which is consistent with the presence of discrete Au nanoparticles and little or no oxidation of the Au nanoparticles. The mass adsorption experiments, carried out using amino functionalised Si_3N_4 'flap' resonators (Figure 1), revealed maximum Au nanoparticle adsorption at pH = 5 (Figure 5), which is in agreement with both the AFM and XPS data. However, the difference between nanoparticle adsorption at pH = 5 and 6 is not as pronounced for the mass adsorption experiments (Figure 5) as it is for the surface coverage obtained by AFM and the Au/Si ratio obtained by XPS (Figure 3).

The pH-dependent adsorption of citrate-passivated Au nanoparticles to chemically modified microresonators with a high Q-factor [4] will be investigated. This will allow the fabrication of highly sensitive mass-detecting MEMS devices.

4. Experimental

All chemicals were obtained from Aldrich unless stated.

4.1. *Preparation of citrate-passivated Au nanoparticles*

Aqueous solutions of citrate-passivated Au nanoparticles were prepared by the method described by Frens [28]. A solution of chloroauric acid (0.01 g, 2.5 mmol in UHQ water)

was heated under reflux for 2 h. Sodium citrate tribasic dihydrate (0.023 g, 0.15 mol) was added to the refluxing chloroauric acid solution and heating continued until there was no further colour change (colourless to red). The solution was allowed to cool to room temperature, centrifuged and the supernatant, containing the nanoparticles, was retained.

4.2. *SAM formation*

4.2.1. *Preparation of Si_3N_4 substrates*

Si/Si_3N_4 substrates (500 nm thick Si_3N_4, Silson Ltd, Northampton, UK) were cleaned and hydroxylated using a method described by Wei et al. [29]. The substrates were rinsed well in EtOH and then in ultra high quality (UHQ) water (resistivity = 18 M Ω cm). The substrates were then immersed in Piranha solution (7 parts H_2SO_4 (98%): three parts H_2O_2 (30%)) at 90–100°C for 30 min and then rinsed thoroughly with UHQ water (Caution: Piranha solution should be handled with extreme caution as it can be explosive upon contact with organic materials).

The substrates were then immersed in NaOH (0.5 M) for 20 min, HCl (0.1 M) for 10 min and NaOH (0.5 M) for 10 min and rinsed with UHQ water between each immersion. The substrates were then rinsed with HCl (0.1 M), water and then purged with $N_{2(g)}$ for 30 min.

The resonating flaps were cut using focused ion beam etching at beam energy of 30 keV in a Dualbeam Strata 235 FIB/SEM system from FEI Co.

4.2.2. *Formation of APTMS SAMs*

The vapour deposition process used for the Si_3N_4 substrate modification with APTMS involves the use of a glass vapour chamber as described previously [22]. The vapour chamber consists of two parts with the top section consisting of a gas tap. The bottom section of the chamber consists of an Al gauze, on which the Si_3N_4 substrates are placed, and an inlet, in which a Subaseal stopper is placed allowing for the injection of APTMS. After the Si_3N_4 substrates have been placed in the chamber, and the top section attached, the chamber was purged with $N_{2(g)}$. The chamber was heated under vacuum, using a heat gun, to encourage desorption of water adsorbed on the inside of the chamber. After the chamber had cooled to room temperature, the APTMS liquid (2 mL) was injected through the Subaseal, whilst the chamber was continuously evacuated for a further 30 min. The gas tap was closed leaving the substrates in an atmosphere of APTMS vapour. After a further 30 min the vacuum was released and the substrates were removed from the chamber. The modification of the Si_3N_4 substrates was performed at a deposition pressure of 168 mbar.

After the vapour deposition the substrates were removed from the chamber and rinsed sequentially in EtOH, $CHCl_3$ and EtOH then cured in a vacuum oven at 120°C for 30 min.

4.3. *Au nanoparticle adsorption studies*

Aqueous solutions of NaOH (1 mM) (Fisher Scientific) and HCl (1 mM) (37%, Fisher Scientific) were prepared and used as stock solutions for the pH adjustment of the citrate-passivated gold nanoparticle solutions. The pH values of the solutions were adjusted by adding minimal amounts of the stock solutions to citrate-passivated gold nanoparticle

solution (4 mL) with the use of a micropipette. The pH values of the solutions were monitored using a digital pH meter (IQ Scientific Instruments). The APTMS-modified silicon nitride surfaces were immersed in one of the pH altered citrate-passivated Au nanoparticle solutions for 2 h and rinsed well with UHQ water and dried under a stream of $N_{2(g)}$.

4.4. *Characterisation*

4.4.1. *AFM*

AFM images were obtained using a MultiMode Scanning Probe Microscope (Veeco) and the images analysed using Nanoscope III v5.12r software. All AFM images were obtained by operating the AFM in non-contact mode with the use of RTESP – Tap300 Metrology Probes (Veeco) (nominal spring constant = 20–80 Nm^{-1}, nominal resonant frequency = 288–328 kHz).

4.4.2. *XPS*

XPS measurements were performed using a VG ESCALab 250 equipped with an Al Kα X-ray source (1486.68 eV), which was operated at 15 kV. Peak fitting and analysis of the data was carried out using Avantage software. All XPS peaks have been fitted by setting the C1s peak to 284.6 eV.

Acknowledgements

This work was supported by the Engineering and Physical Sciences Research Council (EPSRC) (Basic technology) under Grant No. GR/571514/01 and the EU STREP Nano 3-D (NMP4-CT-2005-01406).

References

[1] R. Maboudian, *Surface processes in MEMS technology*, Surf. Sci. Rep. 30 (1998), pp. 207–269.
[2] L.A. Liew, R.A. Saravanan, V.M. Bright, M.L. Dunn, J.W. Daily, and R. Raj, *Processing and characterization of silicon carbon-nitride ceramics: application of electrical properties towards MEMS thermal actuators*, Sens. Actu. A 103 (2003), pp. 171–181.
[3] W. Wang, S. Tatic-Lucic, W.L. Brown, and R. Vinci, *Design of a bidirectional MEMS actuator with high displacement resolution, large driving force and power-free latching*, Microelec. Eng. 85 (2008), pp. 587–598.
[4] B. Boonliang, P.D. Prewett, J. Hedley, J. Preece, and C.A. Hamlett, *A focused-ion-beam micro-paddle resonator for mass detection*, J. Micromech. Microeng. 18 (2008), p. 015021 (4 pp).
[5] N.J. Choi, Y.S. Lee, J.H. Kwak, J.S. Park, K.B. Park, K.S. Shin, H.D. Park, J.C. Kim, J.S. Huh, and D.D Lee, *Chemical warfare agent sensor using MEMS structure and thick film fabrication method*, Sens. Actu. B 108 (2005), pp. 177–183.
[6] D.W. Chun, K.S. Hwang, K. Eom, J.H. Lee, B.H. Cha, W.Y. Lee, D.S. Yoon, and T.S. Kim, *Detection of the Au thin-layer in the Hz per picogram regime based on the microcantilevers*, Sens. Actu. A 135 (2007), pp. 857–862.
[7] K.M. Goeders, J.S. Colton, and L.A. Bottomley, *Microcantilevers: sensing chemical interactions via mechanical motion*, Chem. Rev. 108 (2008), pp. 522–542.

[8] J.W. Gong, Q.F. Chen, W.F. Fei, and S. Seal, *Micromachined nanocrystalline SnO_2 chemical gas sensors for electronic nose*, Sens. Actu. B 102 (2004), pp. 117–125.
[9] P.R. Hauptmann, *Selected examples of intelligent (micro) sensor systems: state-of-the-art and tendencies*, Meas. Sci. & Tech. 17 (2006), pp. 459–466.
[10] N.V. Lavrik, M.J. Sepaniak, and P.G. Datskos, *Cantilever transducers as a platform for chemical and biological sensors*, Rev. Sci. Instrum. 75 (2004), pp. 2229–2253.
[11] P. Li and X.X. Li, *A single-sided micromachined piezoresistive SiO_2 cantilever sensor for ultra-sensitive detection of gaseous chemicals*, J. Micromech. Microeng. 16 (2006), pp. 2539–2546.
[12] D.C. Meier, J.K. Evju, Z. Boger, B. Raman, K.D. Benkstein, C.J. Martinez, C.B. Montgomery, and S. Semancik, *The potential for and challenges of detecting chemical hazards with temperature-programmed microsensors*, Sens. Actu. B 121 (2007), pp. 282–294.
[13] T.E. Mlsna, S. Cemalovic, M. Warburton, S.T. Hobson, D.A. Mlsna, and S.V. Patel, *Chemicapacitive microsensors for chemical warfare agent and toxic industrial chemical detection*, Sens. Actu. B 116 (2006), pp. 192–201.
[14] W. Zhou, A. Khaliq, Y.J. Tang, H.F. Ji, and R.R. Selmic, *Simulation and design of piezoelectric microcantilever chemical sensors*, Sens. Actu. A 125 (2005), pp. 69–75.
[15] Y.C. Li, M.H. Ho, S.J. Hung, M.H. Chen, and M.S.C. Lu, *CMOS micromachined capacitive cantilevers for mass sensing*, J. Micromech. Microeng. 16 (2006), pp. 2659–2665.
[16] O. Lazcka, F.J.D. Campo, and F.X. Munoz, *Pathogen detection: a perspective of traditional methods and biosensors*, Biosens. Bioelec. 22 (2007), pp. 1205–1217.
[17] C.K. O'Sullivan and G.G. Guilbault, *Commercial quartz crystal microbalances - theory and applications*, Biosens. Bioelec. 14 (1999), pp. 663–670.
[18] L.M. Dorozhkin and I.A. Rozanov, *Acoustic wave chemical sensors for gases*, J. Anal. Chem. 56 (2001), pp. 399–416.
[19] J.P. Smith and V. Hinson-Smith, *The new era of SAW devices*, Anal. Chem. 78 (2006), pp. 3505–3507.
[20] T. Zhu, X. Fu, T. Mu, J. Wang, and Z. Liu, *pH-Dependent adsorption of gold nanoparticles on p-aminothiophenol-modified gold substrates*, Langmuir 15 (1999), pp. 5197–5199.
[21] S. Diegoli, P.M. Mendes, E.R. Baguley, S.J. Leigh, P. Iqbal, Y.R. Garcia Diaz, S. Begum, K. Critchley, G.D. Hammond, S.D. Evans, D. Attwood, I.P. Jones, and J.A. Preece, *pH-Dependant gold nanoparticle self-organization on functionalised Si/SiO_2 surfaces*, J. Exp. Nanosci. 1 (2006), pp. 333–353.
[22] C.A.E. Hamlett, K. Critchley, M. Gorzny, S.D. Evans, P.D. Prewett, and J.A. Preece, *Vapour phase formation of amino functionalised Si_3N_4 surfaces*, Surf. Sci. 602 (2008), pp. 2724–2733.
[23] G. Ertas, U.K. Demirok, and S. Suzer, *Enhanced peak separation in XPS with external biasing*, Appl. Surf. Sci. 249 (2005), pp. 12–15.
[24] S. Praharaj, S. Panigrahi, S. Basu, S. Pande, S. Jana, S.K. Ghosh, and T. Pal, *Effect of bromide and chloride ions for the dissolution of colloidal gold*, J. Photochem. Photobio. A 187 (2007), pp. 196–201.
[25] S. Patai, *The Chemistry of the Amino Group*, Interscience Publishers, London, UK, 1968.
[26] B. Wang, R.D. Oleschuk, and J.H. Horton, *Chemical force titrations of amine- and sulfonic acid-modified poly(dimethylsiloxane)*, Langmuir 21 (2005), pp. 1290–1298.
[27] P.W. Atkins, *Physical Chemistry*, 6th ed., Oxford University Press, Oxford, UK, 1998.
[28] G. Frens, *Controlled nucleation for the regulation of the particle size in monodisperse gold suspensions*, Nat. Phys. Sci. 241 (1973), pp. 20–22.
[29] Z.Q. Wei, C. Wang, and C.L. Bai, *Surface imaging of fragile materials with hydrophilic atomic force microscope tips*, Surf. Sci. 467 (2000), pp. 185–190.

Appendix

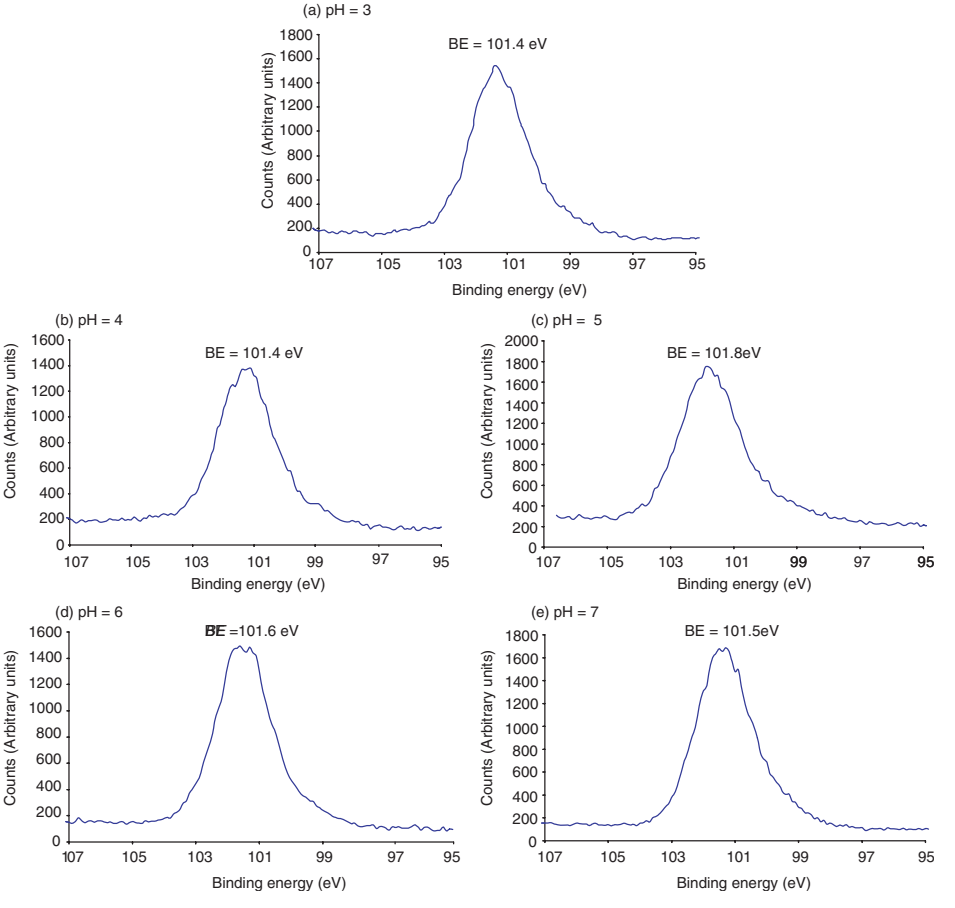

Figure A1. Si 2p spectra of APTMS modified Si_3N_4 substrates after immersion in aqueous solution of citrate-passivated Au nanoparticles for 2 h at five different values of pH. (Binding energy at maximum counts is indicated on each spectrum).

Table A1. The resonant frequencies of the 'flap' resonator before any modification (F_{R1}), after exposure of the resonator to APTMS vapour (F_{R2}) and then after subsequent immersion in citrate-passivated Au nanoparticles (F_{R3}). (The adsorbed mass, calculated from the frequency changes, is also shown).

	Resonant frequencies (kHz)			
pH	F_{R1}	F_{R2}[a]	F_{R3}	Adsorbed mass (ng)
4	25.03	25.03	24.77	4.39
5	25.03	25.03	24.61	7.12
6	25.03	25.03	24.62	6.93

Note: [a]F_{R1} and F_{R2} were found to be the same value. Presumably this is due to the 'flap' resonator not being sensitive enough to detect the mass increase of the adsorption of the APTMS thin film.